Magnesium Spinel Ferrites Development for FDM 3D-Printing Material for Microwave Absorption

Authors:

Vladimir Buzko, Sergey Ivanin, Alexander Goryachko, Ivan Shutkin, Polina Pushankina, Iliya Petriev

Abstract:

The magnesium nanosized ferrite powder with formula MgFe2O4 was synthesized via a pyrochemical sol?gel glycine?nitrate method and annealed consistently at temperatures of up to 1300 °C. The MgFe2O4 ferrite samples' microstructure was studied by SEM and XRD methods. According to the results of the studies, the increase in MgFe2O4 nanoparticles size from about 15 nm to micron-sized particles was observed when increasing annealing temperatures. The DC electrical conductivity of MgFe2O4 also clearly shows the change in conduction behavior of samples with increased calcination temperatures. The electromagnetic microwave properties of micron-sized particles of MgFe2O4 ferrite powder for a 1200 °C annealing temperature were studied for composites in paraffin matrix with produced magnetic filler mass concentration at 40% and 50%. The filament composites of polymer polylactic acid with MgFe2O4 ferrite powder samples were prepared by the FDM 3D-printing process and their microwave-absorbing properties were investigated. The application of developed PLA?MgFe2O4 ferrite filament for fabricating magnetic microwave-absorbing components also was demonstrated.

Article

Magnesium Spinel Ferrites Development for FDM 3D-Printing Material for Microwave Absorption

Vladimir Buzko [1], Sergey Ivanin [1,2], Alexander Goryachko [2], Ivan Shutkin [2], Polina Pushankina [1] and Iliya Petriev [1,3,*]

1 Faculty of Physics and Technology, Kuban State University, 350040 Krasnodar, Russia
2 Center for Advanced Technologies and Nanomaterials, Kuban State Technological University, 350072 Krasnodar, Russia
3 Laboratory of Problems of Stable Isotope Spreading in Living Systems, Southern Scientific Centre of the RAS, 344000 Rostov-on-Don, Russia
* Correspondence: petriev_iliya@mail.ru

Abstract: The magnesium nanosized ferrite powder with formula $MgFe_2O_4$ was synthesized via a pyrochemical sol–gel glycine–nitrate method and annealed consistently at temperatures of up to 1300 °C. The $MgFe_2O_4$ ferrite samples' microstructure was studied by SEM and XRD methods. According to the results of the studies, the increase in $MgFe_2O_4$ nanoparticles size from about 15 nm to micron-sized particles was observed when increasing annealing temperatures. The DC electrical conductivity of $MgFe_2O_4$ also clearly shows the change in conduction behavior of samples with increased calcination temperatures. The electromagnetic microwave properties of micron-sized particles of $MgFe_2O_4$ ferrite powder for a 1200 °C annealing temperature were studied for composites in paraffin matrix with produced magnetic filler mass concentration at 40% and 50%. The filament composites of polymer polylactic acid with $MgFe_2O_4$ ferrite powder samples were prepared by the FDM 3D-printing process and their microwave-absorbing properties were investigated. The application of developed PLA–$MgFe_2O_4$ ferrite filament for fabricating magnetic microwave-absorbing components also was demonstrated.

Keywords: magnesium nanoferrite; composites; microstructure; electrical conductivity; electromagnetic microwave properties; FDM 3D-printing

1. Introduction

Magnesium spinel ferrite $MgFe_2O_4$ is a unique ferrite species with low toxicity and tunable moderate magnetic properties [1–3] performing the random distribution of cations over the available tetrahedral (A) and octahedral [B] sites in the general structure of spinel $MeFe_2O_4$ (Me = two-charged metal ions) ferrites. The degree of inversion in $MgFe_2O_4$ samples and their magnetic properties depends on synthesis methods [4] and sintering temperature [5]. The electromagnetic properties of $MgFe_2O_4$ ferrite samples prepared by sol–gel auto combustion method are different from each other because of their particle size and porosity [2,3,6–10]. The $MgFe_2O_4$ used for constructed miniaturization of microstrip patch antennas used magnetodielectric substrate reduces the size and weight and gives an upgraded S_{11} parameter, bandwidth and directivity as contrasted with planar substrate antennas [11].

Additive manufacturing in fused deposition modelling (FDM) mode, which is a widely used 3D printing low-budget method, is a versatile fabrication method for fast prototyping with the primary goal to decrease the design cycle in a typical R&D process. However, the FDM typically employs only common thermoplastic materials with low glass transition temperature T_g or high dielectric loss at high frequencies, hence limiting their applications to low-power or low-performance microwave devices. Three-D FDM printing is an interesting direction for fabrication of RF and microwave components by utilizing the advantages of the design flexibility, compactness, and fast manufacturing of the next

generation of high-performance 3D-printed RF/microwave devices and antennas operating at RF-wave frequencies [12]. The proposed range of functional microwave devices that might be realized by 3D printing is limited by the current range of developed FDM filament materials. The development of a magnetic composite based on polymer-ferrite composite fiber filaments that are compatible with FDM is a prospective direction. An FDM 3D-printing process with PLA-nanosized $Ni_{0.5}Zn_{0.5}Fe_2O_4$ (35% (wt.)) ferrite-based composite filament for fabricating magnetic and microwave absorption components was demonstrated recently by us [13]. Further, the investigation of 3D-printed NiZn ferrite-ABS composite [14], $Li_{0.44}Zn_{0.2}Fe_{2.36}O_4$/polylactic acid composites [15], $Mn_{0.6}Zn_{0.4}Fe_2O_4$/polylactic acid [16], and Fe-Ni alloy/polylactic acid composites [17] was published.

To understand the effect of $MgFe_2O_4$ particle size on their microwave electromagnetic properties of a comparative study of the annealing effect on microstructure and microwave absorption properties of $MgFe_2O_4$ powders, a prepared sol–gel glycine–nitrate auto combustion method was performed. The glycine–nitrate sol–gel method, followed by calcination of the $MgFe_2O_4$ samples at different temperatures, was proposed as a suitable simple method for the synthesis of spinel nanoferrite powders.

The aim of this work is to evaluate the application of $MgFe_2O_4$ powders produced by glycine–nitrate sol–gel method as magneto-dielectric filler to developed polylactic acid (PLA)-based composites for filament production for FDM 3D-printing. Polylmerized lactic acid or polylactide polymer, which is a readily available engineering modeling plastic, was chosen as the suitable matrix polymer in our investigation due to its well-known ease of printing, low cost, nontoxicity, appropriate biodegradable properties and wide commercial availability. Magnesium ferrite $MgFe_2O_4$ was chosen as magnetic microwave absorption filler due to its well-known ease of production with low cost, nontoxicity, close to ideal ecological properties and good microwave-absorbing properties.

2. Materials and Methods

In this study, polycrystalline nano- and microsized $MgFe_2O_4$ powder samples were prepared in laboratory conditions using a sol–gel glycine–nitrate autocombustion technique. The materials used as precursors were magnesium nitrate hexahydrate $Mg(NO_3)_2 \times 6H_2O$, iron nitrate nonahydrate $Fe(NO_3)_3 \times 9H_2O$ and glycine (all these were purchased from Vecton Ltd., Russian Federation). All of them were of high purity: $Mg(NO_3)_2 \times 6H_2O$ as «pure for analysis» 99%, $Fe(NO_3)_3 \times 9H_2O$ and glycine as «chemically pure grade» with 99.5% and 99.9% purity, respectively. It was known that glycine possesses a high heat of combustion in an oxidized environment [4,18] and its metal-complexing composition provides a suitable sol–gel formation substance for pyrochemical reactions during the course of combustion. Initially the solid magnesium nitrate hexahydrate, iron nitrate nonahydrate and glycine are taken in raw materials in the proposed molar proportion 1:2:6, respectively. The reagent and methods flow chart to synthesize $MgFe_2O_4$ nanosized powder is presented in Figure 1.

Starting chemical materials (both nitrate crystallohydrates as oxidizers and glycine as complexing gelating agent and organic fuel) were carefully dissolved in a beaker with bidistilled water with slow stirring by using a glass rod, and a clear orange solution was obtained. Then they formed a solution that was evaporated on a hot plate in the temperature range of 60 °C to 90 °C, resulting in a thick gel. The gel was kept on a ceramic hot plate for auto combustion and heated in the temperature range of 180 °C to 200 °C so that the resulting gel was self-igniting. The ultradisperse nanocrystalline yellowish-brown $MgFe_2O_4$ powder was formed within a few minutes and after reaction completed and subsequently cooled; the ferrite sample powder was crushed in a ceramic mortar for 5 min. Then, to remove residual impurities, possibly incompletely unreacted starting materials, and increase phase purity and crystallinity, the resulting synthesized powder was then calcined at about 500 °C to 1300 °C with temperature step 100 °C for about 1 h at a heating rate of 20 °C/min in a "Nabertherm Top 16/R + B400" common furnace in an oxygen-containing air medium to produce from light reddish-yellow hue to brown color

shining powder of well-crystallized $MgFe_2O_4$. After the cooling, the calcined magnesium ferrite powder was additionally crushed in a ceramic alumina mortar for 10 min until a homogeneous micro-powder was obtained.
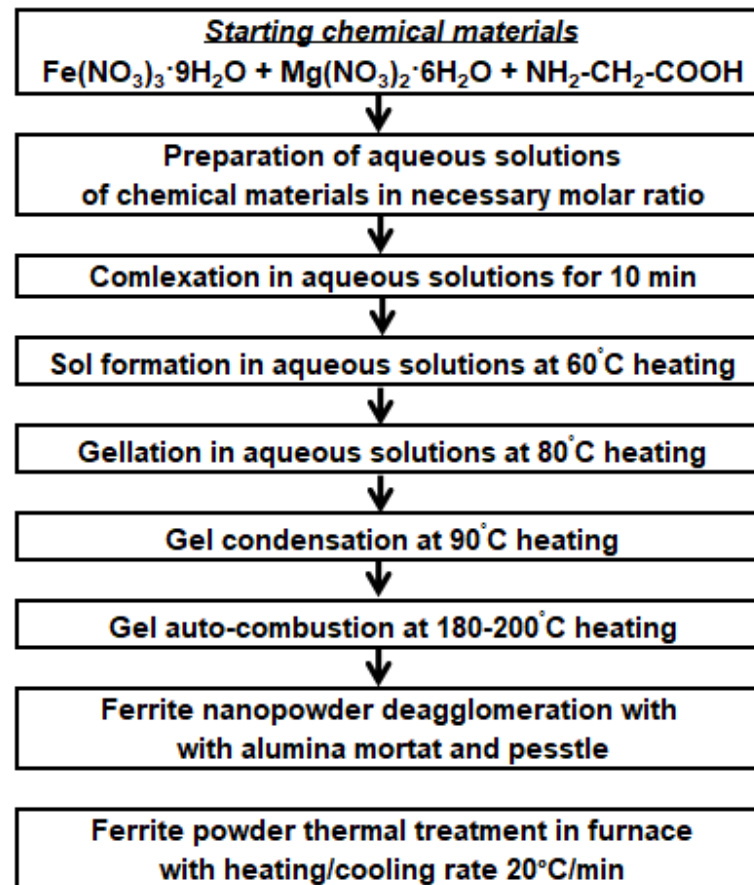

Figure 1. Flow chart to synthesize $MgFe_2O_4$ nanopowder.

Phase evolution of produced $MgFe_2O_4$ powder samples was analyzed by a Shimadzu XRD-7000 X-ray diffractometer (Japan) using monochromatic Cu-Ka radiation (λ = 0.154056 nm) at room temperature in Bragg–Brentano geometry in the range of angles 2θ from $20°$ to $70°$ with a scanning step—$0.05°$ and a spectrum acquisition time of 1 s per point to obtain diffractograms. The average nanocrystallite size in the samples was also calculated from the width of all observed XRD peaks using Scherrer's equation:

$$D_{hkl} = k\lambda / \beta_{hkl}cos\theta$$

where D_{hkl} is the average crystallite size, the coefficient k is 0.9 (for a cubic structure of spinel ferrite), λ is the X-ray wavelength used, β_{hkl} is the intrinsic full width at half maximum of the diffraction line profile, and θ is the position of the principal diffraction peak. The identification of diffraction reflections and the search for crystalline phases in the samples were carried out using the computer program Profex 4.0.0 (Nicola Döbelin, Solothurn, Switzerland) and XPowderX software (ver 2018) (J. Daniel Martín-Islán, Granada, Spain). The density of produced $MgFe_2O_4$ ferrite nanoparticles was determined by the X-ray diffraction method by analyzing the obtained data structural parameters, including the crystal lattice volume.

The morphological features and microstructure of the nanoparticles in produced $MgFe_2O_4$ powder samples depending on the annealing temperature conditions were observed by scanning electron microscope with a Jeol JSM-7500F (Jeol, Tokyo, Japan). The elemental composition of $MgFe_2O_4$ was investigated using the energy-dispersive

analysis method using the INCA X-Sight energy dispersive microanalysis system (Oxford Instruments, Abington, UK) on a scanning electron microscope. Determination of the elemental ratio of $MgFe_2O_4$ samples was performed by collecting statistical data with subsequent averaging and determining the error of measurements.

The DC conductivity of produced $MgFe_2O_4$ powder samples was measured by a two-probe method in plastic tubes with a length of 5.0 mm and an internal diameter of 2.0 mm for a stuffed sample at ~1 ton/cm^2 using a digital resistance meter UT-601 (UNI-T, Dongguan, China) with averaging over 5 measurements.

The electromagnetic characteristics of produced $MgFe_2O_4$ powder samples were investigated by vector network analysis using the Deepace KC901V device (Deepace technology, Dongguan, PRC) in a 10 cm HP-11566A coaxial transmission airline probe (HP, Palo Alto, USA) by the standard method in the form of a composite with concentration 40% and 50% (weight) in paraffin in the form of a pressed toroid with dimensions 3.05 × 7 mm and 5 mm thickness. The choice of the concentration of the investigated $MgFe_2O_4$-paraffin samples and paraffin as a matrix is due to the convenience of comparison with the known data on the previously investigated different types of microwave-absorbing fillers. Calculation of the electromagnetic characteristics (complex permeability $\mu = \mu' + i\mu''$ and permittivity $\varepsilon = \varepsilon' + i\varepsilon''$) of the samples from the measured scattering parameters S_{11} and S_{21} were carried out by the Nicolson–Ross–Weir method [19].

The $MgFe_2O_4$ with polylactic acid (FDplast Company, Moscow, Russian Federation) composite filament was prepared by ball milling mixing in an alumina jar and balls and subsequent melt extrusion (Wellzoom Desktop Extruder Line II, Shanghai, China) with control of the nozzle temperature in the range 200–210 °C. Approximately, the self-made 2–3 m of $MgFe_2O_4$-PLA composite filament of 1.75 mm diameter with standard deviation of 0.02–0.03 mm was made with different samples of calcined $MgFe_2O_4$ powders. The $MgFe_2O_4$–PLA composites were prepared by fused deposition modeling by the FlashForge Creator Pro 3D printer (Zhejiang Flashforge 3D Technology Co., Jinhua, China) using concentric rings print style with 100% filling factor with the corresponding settings: 200 °C titanium alloy nozzle temperature and 80 °C printed bed temperature.

The DSC analysis of prepared $MgFe_2O_4$-PLA samples allowed investigating the transition temperatures for melting and crystallization, as well as glass-transition temperatures. The heat-flux DSC 204 F1 Phoenix (NETZSCH-Gerätebau GmbH, Selb, Germany) setups were used. Microwave absorption performances of the 3D-printed $MgFe_2O_4$–PLA sample were evaluated based on the measured reflection loss (RL) values data for a 3.05 × 7 mm composite toroid with thickness of 10 mm in an HP-11566A coaxial transmission airline probe.

3. Results

3.1. Electron Microscopy

In order to study the effect of calcination temperature on the morphology of $MgFe_2O_4$ particles in their powder samples, the scanning electron microscopy investigation was carried out. The morphologies of $MgFe_2O_4$ specimens calcined at temperatures from 500 °C to 1300 °C are shown in Figure 2.

3.2. XRD Analysis

The XRD patterns of the calcined $MgFe_2O_4$ samples (Figure 3) show that as the calcination temperature increases, the associated diffraction peaks become sharper and more intense, indicating an improvement in crystalline quality of produced ferrite with calcination temperature increase.

3.3. DC Electrical Conductivity

Figure 4 shows a graph of the dependence of the annealing temperature on electrical conductivity of $MgFe_2O_4$ powders for direct current condition.
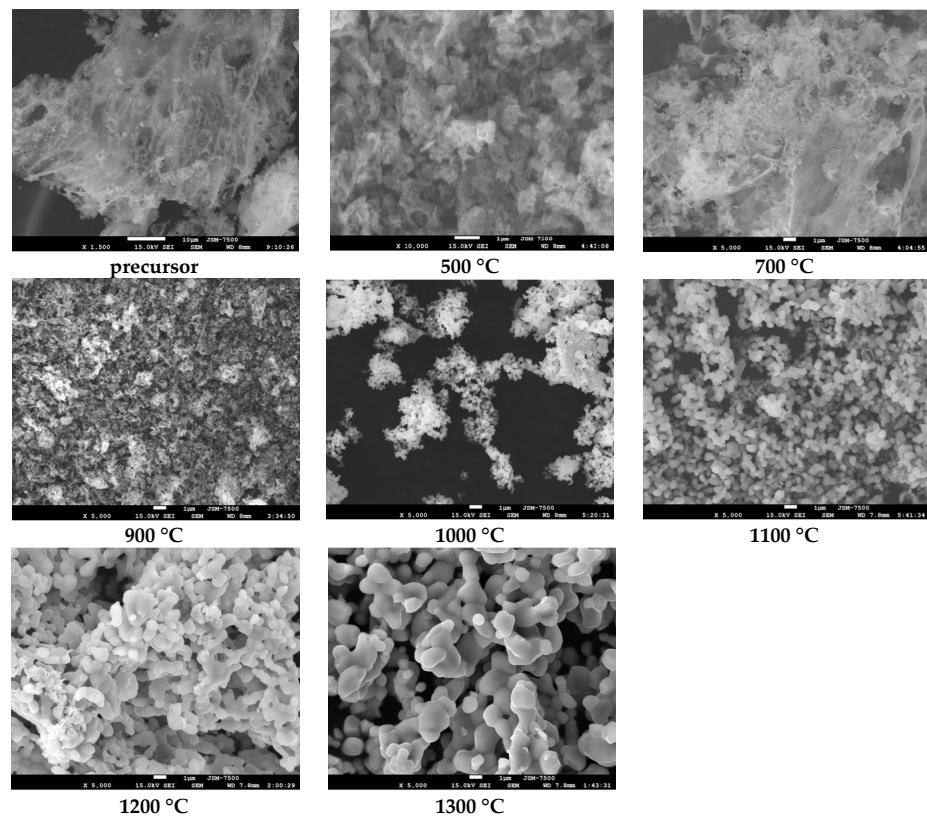
Figure 2. SEM images of the MgFe$_2$O$_4$ powders calcined at the various temperatures.
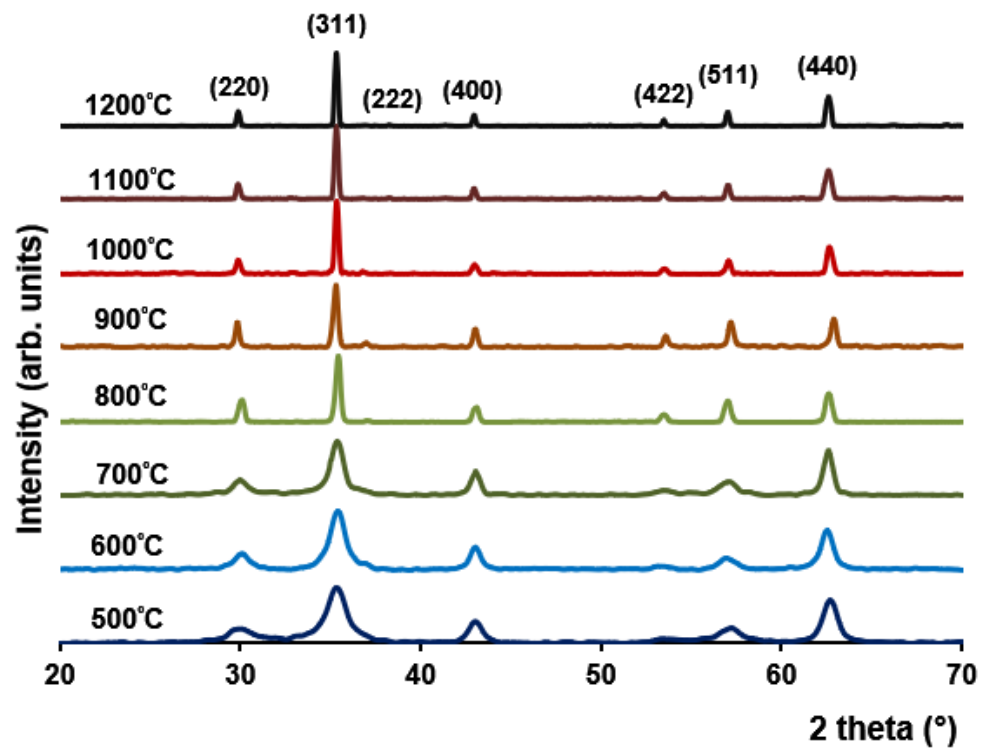

Figure 3. X-ray diffraction results for the MgFe$_2$O$_4$ samples following calcination at the various temperatures.
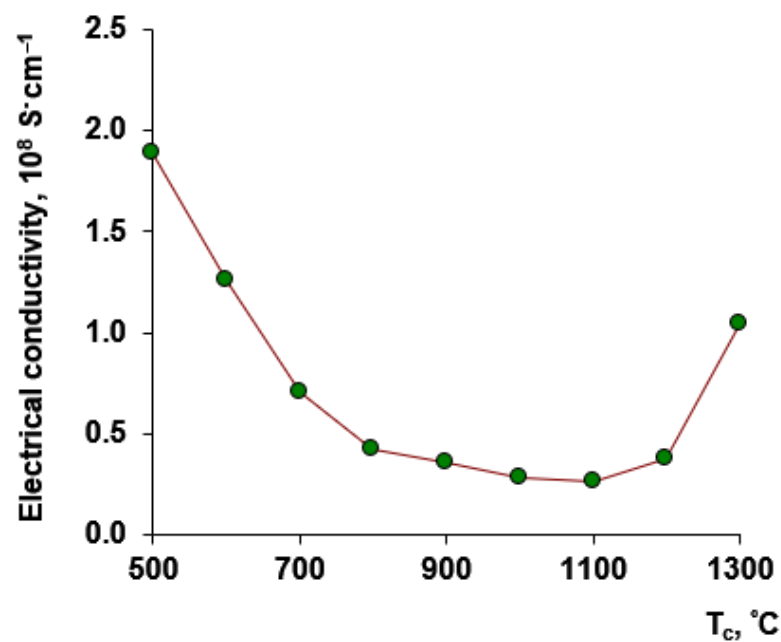
Figure 4. DC electrical conductivity of $MgFe_2O_4$ powders for samples calcined at different temperatures.

3.4. EDX Analysis

Figure 5 shows the results of energy-dispersive X-ray elemental microanalysis of $MgFe_2O_4$ powder calcined at 1200 °C.
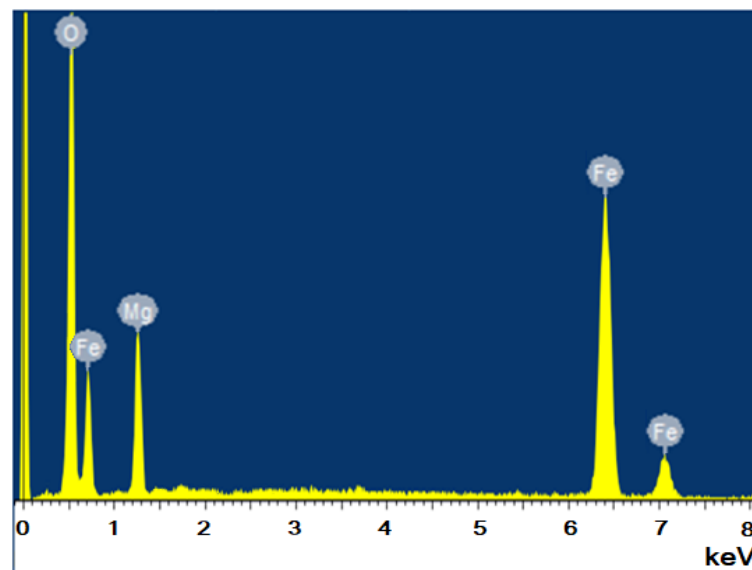

Figure 5. EDX spectrum of $MgFe_2O_4$ sample calcined at 1200 °C.

3.5. VNA Measurement $MgFe_2O_4$–Paraffin Composites

The electromagnetic characteristics of the manufactured $MgFe_2O_4$–paraffin composites with a mass concentration of magnesium ferrite particles of 40% and 50% were investigated by the VNA method. The EM frequency dependence of calculated complex permeability and permittivity with corresponding loss tangents for $MgFe_2O_4$–parrafin composite and parrafin and PLA polymer matrix are in Figures 6 and 7.
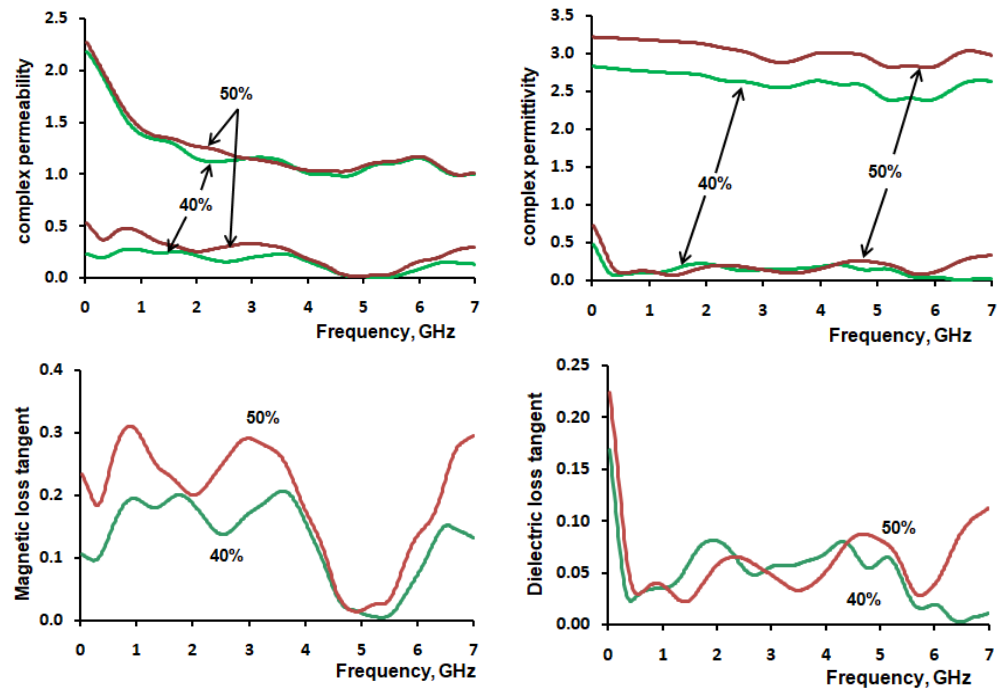
Figure 6. The complex permeability, complex permittivity, magnetic loss and dielectric loss tangent of $MgFe_2O_4$–paraffin composite.
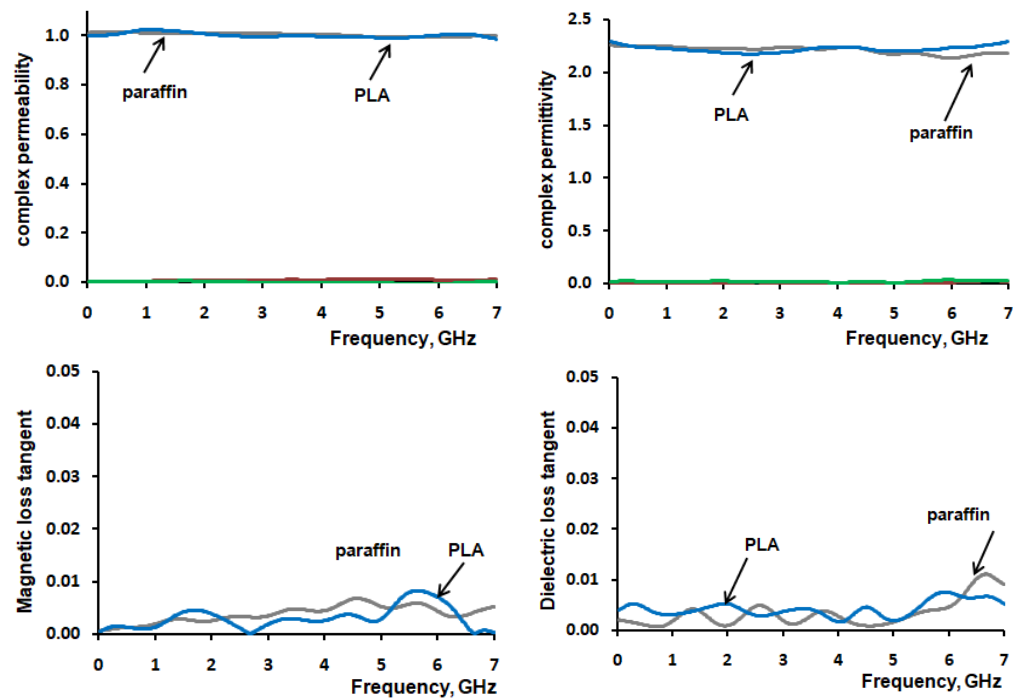

Figure 7. The complex permeability, complex permittivity, magnetic loss and dielectric loss tangent of paraffin and PLA polymer.

3.6. 3D FDM Printing $MgFe_2O_4$–PLA

Two samples of composite materials were made based on the obtained $MgFe_2O_4$ micro-powder at an annealing temperature of 1200 °C and PLA polylactide with a concentration of magnetic filler particles of 40% and 50%, respectively. The choice of $MgFe_2O_4$ powder at an annealing temperature of 1200 °C as a filler is due to the suitable shape and size of its microparticles, without a large number of agglomerates that can significantly complicate

the 3D printing process due to the strong friction and wear in the heated extrusion nozzle. The DSC data for investigated MgFe$_2$O$_4$–PLA composites are shown in Figure 8 and Table 1.
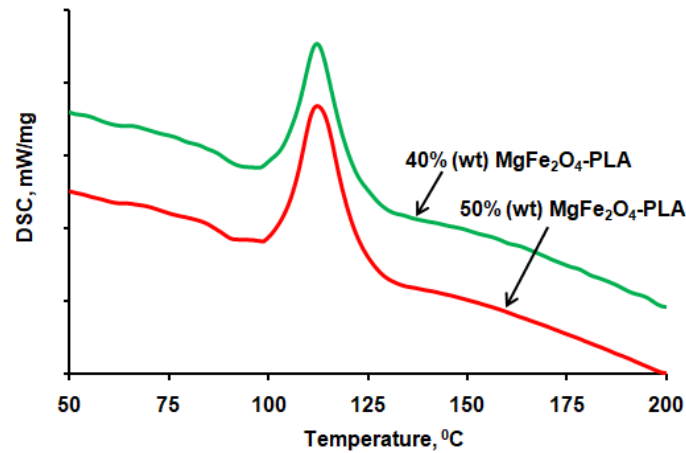

Figure 8. DSC thermograms of MgFe$_2$O$_4$–PLA composites.

Table 1. DSC data of MgFe$_2$O$_4$-PLA composites.

Sample	T_m, °C	T_c, °C	T_g, °C
40% (wt.) MgFe$_2$O$_4$-PLA	112.1	97.8	81.5
50% (wt.) MgFe$_2$O$_4$-PLA	111.7	98.7	90.2

T_m—melting temperature; T_c—crystallization temperature; T_g—glass transition temperature.

According the data from Table 1, low printing temperature and practically observed good observed layer adhesion make the developed MgFe$_2$O$_4$–PLA composites suitable good material for 3D FDM printing.

It was obvious that the ferrite fraction in plastic composites for 3D printing is desired to be as high as possible to provide the highest magnetic permeability across a printed component. However, the MgFe$_2$O$_4$ fraction in PLA plastic must be low enough so as to enable the material to exit the heated extrusion nozzle of common 3D printers. We carried out optimization between composite filament extrusion production, printing parameters, and reliable operation in the FDM 3D-printing process of MgFe$_2$O$_4$–PLA composite filament. The suitable maximum fraction is 40% weight MgFe$_2$O$_4$ ferrite. The COMPO micro-image of the PLA–40% weight MgFe$_2$O$_4$ composite microstructure in Figure 9 reflects the relative homogeneous distribution of MgFe$_2$O$_4$ microparticles in PLA polymer matrix.
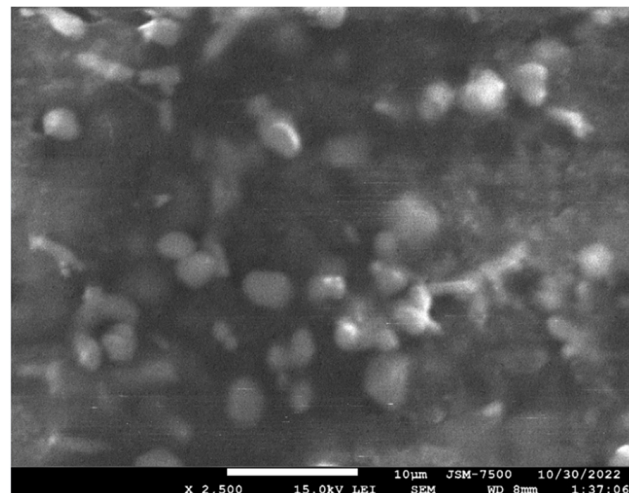

Figure 9. COMPO image of the PLA–40% weight MgFe$_2$O$_4$ composite.

We make note that at higher ferrite micropowder fractions, the filament tends towards brittle behavior in feeding and becomes difficult to print [13]. The printability of the composite filament was assessed by printing simple blocks using the FDM process. The composite filament is driven by a stepper motor into a temperature-controlled nozzle, and molten material is extruded and deposited onto the build platform in a layer according to the pre-programmed pattern.

3.7. VNA Measurement $MgFe_2O_4$–PLA Composites

The measured reflection losses for a 3D-printed sample of the composition of 40% (wt.) $MgFe_2O_4$–PLA and pure PLA polymer at a thickness of 10 mm are shown in Figure 10.
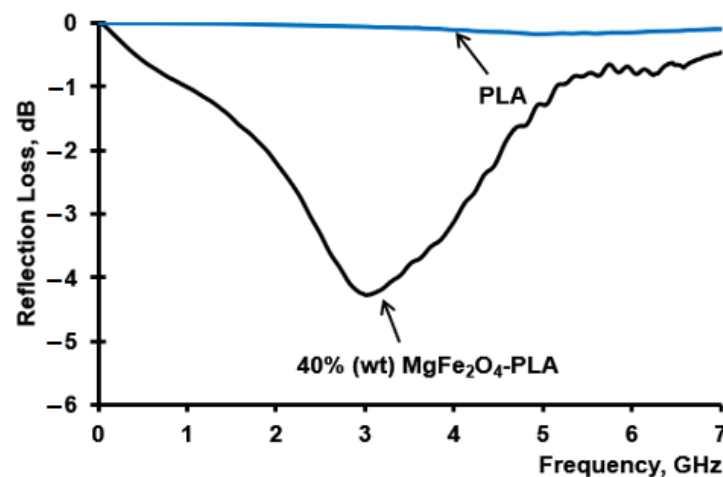

Figure 10. The measured reflection loss of 40% (wt.) $MgFe_2O_4$–PLA and pure PLA polymer FDM 3D-printed samples.

4. Discussion

SEM images show that the non-calcined samples (precursor) of $MgFe_2O_4$ consist of very small particles with average grain size of 15 ± 5 nm. It should be noted that the main morphological changes in studied $MgFe_2O_4$ samples were observed at temperatures above 700 °C, with a change in the shape of particles from an amorphous loose network to close-to-spherical nanoparticles. In the course of our research, it was found that highly ordered $MgFe_2O_4$ nanoparticles with an average size of 50–60 nm are formed at 700–800 °C. As can be seen from the presented data, a change in the treatment temperature leads to a change in the morphological features of nanoparticles related primarily to their enlargement and formation of large agglomerates at high temperatures (above 900 °C) resulting from the sintering of $MgFe_2O_4$ nanoparticles. The $MgFe_2O_4$ specimen sintered at 1100 °C (Figure 2) exhibits small equiaxed particles with average size of about 400 ± 100 nm, although larger agglomerates are also seen. Meanwhile, pronounced grain growth of $MgFe_2O_4$ particles is seen at the sintering temperatures of 1200 °C and 1300 °C (Figure 2). The $MgFe_2O_4$ specimen sintered at 1300 °C is composed of uniform coarse structure with a well-clear crystalline microstructure having very small numbers of small particles. The average grain size for the $MgFe_2O_4$ powder specimen calcined at 1200 °C was about 1.1 ± 0.5 μm. An average grain size at 1300 °C of 2.1 ± 0.7 μm was obtained for the $MgFe_2O_4$ sample calcined at 1300 °C. An increase in grain size, followed by the formation of agglomerates, leads to a decrease in the specific surface area of $MgFe_2O_4$ powders, which may positively affect the mixing characteristics of ferrite powders with polymer matrix.

All the observed diffraction peaks for the $MgFe_2O_4$ samples (Figure 3) were compared with standard diffraction lines of magnesium spinel ferrite, JCPDS Card No. 88-1943. The most prominent diffraction peak is centered at $2\theta = 35.3$–$35.4°$ and corresponds to crystal plane (311), which is a characteristic peak of $MgFe_2O_4$ spinel structure. The other peaks are also assigned to spinel cubic structure (Figure 3) with Miller indices of (111), (220), (311),

(222), (400), (422), (511) and (440). It is established that all the produced $MgFe_2O_4$ samples correspond to cubic phase with symmetry group $Fd\overline{3}m$. The lattice parameter (a) of the $MgFe_2O_4$ sample sintered at 1000 °C was found to be 8.4004 Å with corresponding X-ray density about 4.52 g/cm^3, consistent with the literature. The a value for stoichiometric $MgFe_2O_4$ usually ranges between 8.38–8.40 Å [20,21] and is consistent with our value.

The XRD graphs for investigated $MgFe_2O_4$ samples reveal decrease in full width half maxima (FWHM) with the increase in sintering temperature. The $MgFe_2O_4$ grain size for powder samples calcined at a temperature range from 500 to 1000 °C was obtained from Scherrer's formula using FWHM and peak position of the sample after correcting for instrumental broadening and is presented in Table 2.

Table 2. The grain size from XRD for $MgFe_2O_4$ samples calcined at different temperatures.

Calcination Temperature, °C	500	600	700	800	900	1000	1100	1200
D_m, nm	10.2	11.8	15.1	29.7	31.6	48.0	57.3	74.1

The grain size was estimated to be around 10.2 nm for the ultra-disperse $MgFe_2O_4$ sample calcined at 500 °C. With the increase in sintering temperature, the grain size of $MgFe_2O_4$ increases dramatically and reached the value of around 74.1 nm for crystallites in the $MgFe_2O_4$ sample calcined at 1200 °C. For the further increase in sintering temperature to 1300 °C, it was not possible to adequately measure grain size in the prepared $MgFe_2O_4$ sample with X-ray diffraction due to instrumental broadening.

It is widely known that since Mg^{2+} ions are non-magnetic, the magnetic moment of $MgFe_2O_4$ is derived from the particular type of cation distribution. It is a known fact that there is a remarkable effect of initial particle size on bulk magnetic properties of sintered product. According to published data, $MgFe_2O_4$ spinel ferrite is partly inverse and partly normal and is, therefore, one of the most interesting ferrite spinels [3,4]. At room temperature, $MgFe_2O_4$ has an inverse spinel structure in which the divalent and half of the trivalent ions are arranged in the octahedral positions and the remaining trivalent ions fill the tetrahedral positions with the degree of inversion of the structure about 0.90 [21]. This means that its structure is very close to the perfectly inverse one. An increase in temperature above the annealing temperature of 600 °C leads to an increase in the intensity of these reflexes, which indicates an ordering of the crystal structure. At around the temperature of 700 K, the value of $MgFe_2O_4$ inversion degree begins to drop and at 1400 K reaches the value of 0.70 [3,4]. As indicated by literature data, the beginning of inversion in the structure of $MgFe_2O_4$ occurs within the 573–723 K temperature range [21–23].

The measured DC electrical conductivity of $MgFe_2O_4$ compacted powder samples obtained at different calcination temperatures (Figure 4) also clearly shows the change in electrical conduction behavior of samples with increased calcination temperatures. The minimum of DC electrical conductivity for $MgFe_2O_4$ powder samples was observed at a 1000–1100 °C calcination temperature range. Possibly this result reflected the grain growth and coalescence of $MgFe_2O_4$ nanoparticles. Our data are in accordance with observation that $MgFe_2O_4$ is a soft magnetic semiconductor and possesses high resistivity [24].

The $MgFe_2O_4$ powder sample calcined at 1200 °C was analyzed by X-ray elemental microanalysis. In the EDX spectra (Figure 5), no impurity elements are seen, except Mg, Fe and O. The calculated atomic ratio of Mg and Fe elements is approximately 1:2.

It was found that the attenuation of electromagnetic waves in nanosized $MgFe_2O_4$ based materials above 1000 MHz mainly comes from magnetic loss [25,26], and in the frequency range of 7–18 GHz the $MgFe_2O_4$ was the dielectric loss materials [27]. We found that in our case of used microsized $MgFe_2O_4$ powder, the composite $MgFe_2O_4$_paraffin materials can dissipate EM-waves from magnetic loss in the 0.5–4 GHz range (Figure 6).

The calculated dielectric constant and loss tangent of the used paraffin and PLA matrix presented in Table 3.

Table 3. Calculated dielectric constant and loss tangent of the paraffin and PLA.

Material	Dielectric Constant	Magnetic Loss Tangent	Dielectric Loss Tangent
Paraffin	2.211 ± 0.029	0.004 ± 0.002	0.0023 ± 0.012
PLA-printed	2.220 ± 0.027	0.003 ± 0.002	0.0043 ± 0.015

According to collected data in Figure 7, the prepared by FDM 3D-printing process with 40% (wt.) $MgFe_2O_4$–PLA materials have moderate microwave absorption properties in the 4G cell phone communication range. The observed microwave absorption peak resonance is located at a frequency of about 3.0 GHz. Thus, we can suggest that FDM 3D-printed 40% (wt.) $MgFe_2O_4$–PLA composites are appropriate for application as magnetodielectric ferrite substrates for printed and microstrip antenna miniaturization with enhanced radiation performance attractive for practical applications such as Bluetooth and Wi-Fi.

Further, we can conclude that as a microwave-absorbing filler, produced $MgFe_2O_4$ powder is inferior to domestic magnetic microwave-absorbing materials previously studied by us such as magnetic microspheres [28], Fe-Si-Al alloy micropowders [29] or ferrite powders of spinel series [13,30–33] (Table 4). However, $MgFe_2O_4$ is a practical, easily produced, low-cost, ecological microwave-absorbing material.

Table 4. Microwave absorption characteristics of magnetodielectric composites.

Material	RL_{max}, dB	Frequency at RL_{max}, GHz	Reference
40% (wt.) $MgFe_2O_4$-PLA, 10 mm	−4.28	3.00	This work
35% (wt.) $Ni_{0.5}Zn_{0.5}Fe_2O_4$-PLA, 10 mm	−4.49	4.22	[13]
40% (wt.) $Mn_{0.6}Zn_{0.4}Fe_2O_4$-PLA, 7.4 mm	−7.2	5.7	[16]
40% (wt.) FeNi50-PLA, 3.0 mm	−6.2	12.7	[17]
50% (wt.) magnetic microspheres-paraffin 10 mm	−6.55	3.38	[28]
40% (wt.) Fe-Si-Al alloy micropowder-paraffin, 5 mm	−16.76	4.57	[29]
50% (wt.) $Co_{0.5}Zn_{0.5}Fe_2O_4$-paraffin, 10 mm	−9.09	4.26	[32]
50% (wt.) $Ni_{0.5}Zn_{0.5}Fe_2O_4$-paraffin, 10 mm	−7.58	4.42	[33]

RL_{max}—maximal value of microwave absorption in peak of measured reflection loss; **Frequency at RL_{max}**—frequency microwave absorption peak of measured reflection loss.

Thus, an additive manufacturing FDM 3D-printing process with self-developed $MgFe_2O_4$–PLA composite filament for fabricating magnetic microwave-absorbing components was also demonstrated. Therefore, the investigated 3D-printed $MgFe_2O_4$–PLA composite prepared based on FDM has moderate microwave-absorbing properties and good bearing capacity and it is a promising microwave-absorbing material for 3D printing by the FDM method.

5. Conclusions

Magnesium spinel-type ferrite $MgFe_2O_4$ magnetic powder material was successfully synthesized by the glycine–nitrate sol–gel auto-combustion method. Crystallinity and grain size of the $MgFe_2O_4$ powder samples products increase with the increase in sintering temperatures. A single cubic phase of $MgFe_2O_4$ was achieved after calcinations at 900 °C for 1 h. X-ray diffraction study confirmed the formation of a pure phase $MgFe_2O_4$ space group of $Fd\overline{3}m$ (cubic spinel) with a parameter of a = 8.4004 Å at 1000 °C. The DC electrical conductivity of $MgFe_2O_4$ also clearly shows the change in conduction behavior of samples with increase calcination temperatures and reflects high resistivity of $MgFe_2O_4$. The electromagnetic microwave properties of micron-sized particles of $MgFe_2O_4$ ferrite powder for 1200 °C annealing temperatures was studied for composites in paraffin with produced magnetic filler mass concentration from 40% and 50%. In this regard, we can conclude that $MgFe_2O_4$-based polymer composite materials can effectively dissipate EM-waves from

magnetic loss in the 0.5–4 GHz range. The filament composites of polylactic acid with MgFe$_2$O$_4$ ferrite powder samples were prepared by the FDM 3D-printing process and their microwave-absorbing properties were investigated. The application of developed PLA–MgFe$_2$O$_4$ ferrite filament for fabricating magnetic microwave-absorbing components also was demonstrated.

References

1. Aliyan, N.; Mirkazemi, S.M.; Masoudpanah, S.M.; Akbari, S. The effect of post-calcination on cation distributions and magnetic properties of the coprecipitated MgFe2O4 nanoparticles. *Appl. Phys. A* **2017**, *123*, 446. [CrossRef]
2. Mahato, D.K.; Majumder, S.; Banerjee, S. Large polaron tunneling, magnetic and impedance analysis of magnesium ferrite nanocrystallite. *Appl. Surf. Sci.* **2017**, *413*, 149–159. [CrossRef]
3. Araújo, J.; Araujo-Barbosa, S.; Souza, A.; Iglesias, C.; Xavier, J.; Souza, P.; Cid, C.P.; Azevedo, S.; da Silva, R.; Correa, M.; et al. Tuning structural, magnetic, electrical, and dielectric properties of MgFe2O4 synthesized by sol-gel followed by heat treatment. *J. Phys. Chem. Sol.* **2021**, *154*, 110051. [CrossRef]
4. Zampiva, R.Y.S.; Kaufmann, C.G., Jr.; Alve, A.K.; Bergmann, C.P. Influence of the Fuel Composition and the Fuel/Oxidizer Ratio on the Combustion Solution Synthesis of MgFe$_2$O$_4$ Catalyst Nanoparticles. *FME Trans.* **2018**, *46*, 157–164.
5. Gerle, A.; Piotrowski, J.; Podworny, J. The Influence of Order in the Cation Sublattice of MgAl$_2$O$_4$, MgCr$_2$O$_4$ and MgFe$_2$O$_4$ Spinels on the Kinetics of Topochemical Reactions with Sulphur Oxides. *J. Ceram. Sci. Technol.* **2017**, *8*, 183–192.
6. De Hoyos-Sifuentes, D.H.; Reséndiz-Hernández, P.J.; Díaz-Guillén, J.A.; Ochoa-Palacios, R.M.; Altamirano-Guerrero, G. Synthesis and characterization of MgFe$_2$O$_4$ nanoparticles and PEG-coated MgFe$_2$O$_4$ nanocomposite. *J. Mater. Res. Technol.* **2022**, *18*, 3130–3142. [CrossRef]
7. Kaur, N.; Kaur, M. Comparative studies on impact of synthesis methods on structural and magnetic properties of magnesium ferrite nanoparticles. *Process. Appl. Ceram.* **2014**, *8*, 137–143. [CrossRef]
8. Hussein, S.I.; Elkady, A.S.; Rashad, M.M.; Mostafa, A.G.; Megahid, R.M. Structural and magnetic properties of magnesium ferrite nanoparticles prepared via EDTA-based sol–gel reaction. *J. Magn. Magn. Mater.* **2015**, *379*, 9–15. [CrossRef]
9. Durrani, S.K.; Naz, S.; Mehmood, M.; Nadeem, M.; Siddique, M. Structural, impedance and Mössbauer studies of magnesium ferrite synthesized via sol–gel auto-combustion process. *J. Saudi Chem. Soc.* **2017**, *21*, 899–910. [CrossRef]
10. Easwari, M.; Jesurani, S. Synthesis & Magnetic Properties of Magnesium Ferrite (MgFe$_2$O$_4$) Nanoparticles Via Sol Gel Method. *Int. Res. J. Eng. Technol.* **2017**, *4*, 110–113.
11. Naidu, V.; Seeni, S.M.; Maraikkayar, M.A.; Sivaranjani, S.; Kalpana, M.; Jeeva, R.K.; Pandian, S. Engineered meta magneto dielectric substrate for microstrip patch antenna miniaturization with reduced return loss. *Int. J. Appl. Eng.* **2015**, *10*, 30474–30479.
12. Lee, C.-K.; McGhee, J.; Tsipogiannis, C.; Zhang, S.; Cadman, D.; Goulas, A.; Whittaker, T.; Gheisari, R.; Engstrom, D.; Vardaxoglou, J.; et al. Evaluation of Microwave Characterization Methods for Additively Manufactured Materials. *Designs* **2019**, *3*, 47. [CrossRef]
13. Shamray, I.I.; Buz'Ko, V.Y.; Goryachko, A.I. Changes in the Structure and Properties of Nickel-Zinc Spinel Nanoferrites Series for 3D-Printing. *IOP Conf. Ser. Mater. Sci. Eng.* **2020**, *969*, 012101. [CrossRef]
14. Wang, Y.; Castles, F.; Grant, P.S. 3D Printing of NiZn ferrite/ABS Magnetic Composites for Electromagnetic Devices. *MRS Proc.* **2015**, *1788*, 29–35. [CrossRef]

15. Qian, Y.; Yao, Z.; Lin, H.; Zhou, J. Mechanical and microwave absorption properties of 3D-printed Li0.44Zn0.2Fe2.36O4/polylactic acid composites using fused deposition modeling. *J. Mater. Sci. Mater. Electron.* **2018**, *29*, 19296–19307. [CrossRef]

16. Xicong, Y.; Qi, G.; Enyi, H.; Chao, Y.; Bin, O.; Peng, Y.; Haihua, W. Mechanical and microwave absorbing properties of Mn-Zn ferrite/polylactic acid composites formed by fused deposition modeling. *Acta Mater. Compos. Sin.* **2022**, *10*, 1–13.

17. Haihua, W.; Zhenglang, H.; Yutian, L.; Peng, Q.; Li, L.; Jianxin, Z. Electromagnetic absorption properties and mechanical properties of Fe-Ni alloy/polylactic acid composites fabricated by fused deposition modeling. *Acta Mater. Compos. Sin.* **2022**, *39*, 172–182.

18. Khot, V.M.; Salunkhe, A.B.; Phadatare, M.R.; Pawar, S.H. Formation, microstructure and magnetic properties of nanocrystalline $MgFe_2O_4$. *Mater. Chem. Phys.* **2012**, *132*, 782–787. [CrossRef]

19. Rothwell, E.J.; Frasch, J.L.; Ellison, S.M.; Chahal, P.; Ouedraogo, R.O. Analysis of the Nicolson-Ross-Weir Method for Characterizing the Electromagnetic Properties of Engineered Materials. *Prog. Electromagn. Res. C* **2016**, *157*, 31–47. [CrossRef]

20. Antao, S.M.; Hassan, I.; Parise, J.B. Cation ordering in magnesioferrite, $MgFe_2O_4$, to 982 °C using in situ synchrotron X-ray powder diffraction. *Am. Mineral.* **2005**, *90*, 219–228. [CrossRef]

21. Gateshki, M.; Petkov, V.; Pradhan, S.K.; Vogt, T. Structure of nanocrystalline $MgFe_2O_4$ from X-ray diffraction, Rietveld and atomic pair distribution function analysis. *J. Appl. Cryst.* **2005**, *38*, 772–779. [CrossRef]

22. O'Neil, H.; Annersten, H.; Virgo, D. The temperature dependence of the cation distribution in magnesioferrite ($MgFe_2O_4$) from powder XRD structural refinements and Mössbauer spectroscopy. *Am. Mineral.* **1992**, *77*, 725–740.

23. Harrison, R.J.; Putnis, A. Determination of the mechanism of cation ordering in magnesioferrite ($MgFe_2O_4$) from the time and temperature-dependence of magnetic susceptibility. *Phys. Chem. Miner.* **1999**, *26*, 322–332. [CrossRef]

24. Tian, N.; Wang, J.W.; Li, F.; Mei, Z.; Lu, Z.X.; Ge, L.L.; You, C.Y. Enhanced microwave absorption of Fe flakes with magnesium ferrite cladding. *J. Magn. Magn. Mater.* **2012**, *324*, 4175–4178. [CrossRef]

25. Wang, Q.; Wang, X.; Zhuang, J. Synthesis for powder of nano-$MgFe_2O_4$/Fe_2O_3 by citrate sol-gel and absorbs characteristic of electromagnetic wave. *J. Func. Mater.* **2005**, *36*, 1839–1841.

26. Chen, W.; Liu, Q.; Zhu, X.; Fu, M. One-step in situ growth of magnesium ferrite nanorods on graphene and their microwave-absorbing properties. *Appl. Organomet. Chem.* **2018**, *32*, e4017. [CrossRef]

27. Tang, H.; Xu, B.; Wang, S.; Zhang, Y.G. $MgFe_2O_4$ nanoparticles preparation and its electromagnetic properties. *J. Func. Mater.* **2013**, *44*, 776–779.

28. Vyzulin, S.A.; Buz'ko, V.Y.; Kalikintseva, D.A.; Goryachko, A.I.; Sarin, L.I.; Kolantsov, O.A.; Syr'ev, N.E. Magnetic and dielectric properties of composites based on magnetic microspheres. *J. Phys. Conf. Ser.* **2019**, *1389*, 012161. [CrossRef]

29. Goryachko, A.I.; Ivanin, S.N.; Buz'ko, V.Y. Electromagnetic properties of composite materials based on Nd-compound modified Fe-Si-Al alloy. *IOP Conf. Ser. Mater. Sci. Eng.* **2020**, *969*, 012019. [CrossRef]

30. Vyzulin, S.A.; Miroshnichenko, E.L.; Kalikintseva, D.A.; Buz'ko, V.Y. Investigation of microwave absorption properties of nanosized nickel-zinc ferrites powders. In Proceedings of the 2017 Radiation and Scattering of Electromagnetic Waves (RSEMW), Divnomorskoe, Russia, 26–30 June 2017; pp. 152–154.

31. Vyzulin, S.A.; Kalikintseva, D.A.; Miroshnichenko, E.L.; Buz'Ko, V.Y.; Goryachko, A.I. Microwave Absorption Properties of Nickel–Zinc Ferrites Synthesized by Different Means. *Bull. Russ. Acad. Sci. Phys.* **2018**, *82*, 943–945. [CrossRef]

32. Goryachko, A.I.; Ivanin, S.N.; Buzko, V.Y. Synthesis, Microstructural and Electromagnetic Characteristics of Cobalt-Zinc Ferrite. *Condens. Matter Interphas.* **2020**, *22*, 446–452. [CrossRef] [PubMed]

33. Buz'Ko, V.Y.; Shamrai, I.I.; Ryabova, M.Y.; Kireeva, G.V.; Goryachko, A.I. Properties of Nickel Zinc Ferrite Nanopowders Prepared by Different Methods. *Inorg. Mater.* **2021**, *57*, 38–43. [CrossRef]